REGULAR ARTICLE

Chemical bonding in "early–late" transition metal complexes [(H₂N)₃M–M′(CO)₄] (M = Ti, Zr, Hf; M′ = Co, Rh, Ir)

Andreas Krapp · Gernot Frenking

Abstract Quantum chemical DFT calculations at the BP86/TZ2P level have been carried out for the complex [HSi(SiH₂NH)₃Ti–Co(CO)₄], which is a model for the experimentally observed compound [MeSi{SiMe₂N(4-MeC₆H₄)}₃Ti–Co(CO)₄] and for the series of model systems [(H₂N)₃M–M′(CO)₄] (M = Ti, Zr, Hf; M′ = Co, Rh, Ir). The Ti–Co bond in [HSi(SiH₂NH)₃Ti–Co(CO)₄] has a theoretically predicted BDE of D_e = 59.3 kcal/mol. The bonding analysis suggests that the titanium atom carries a large positive charge, while the cobalt atom is nearly neutral. The covalent and electrostatic contributions to the Ti–Co attraction have similar strength. The Ti–Co bond can be classified as a polar single bond, which has only little π contribution. Calculations of the model compound (H₂N)₃Ti–Co(CO)₄ show that the rotation of the amino groups has a very large influence on the length and on the strength of the Ti–Co bond. The M–M′ bond in the series [(H₂N)₃M–M′(CO)₄] becomes clearly stronger with Ti < Zr < Hf, while the differences between the bond strengths due to change of the atoms M′ are much smaller. The strongest M–M′ bond is predicted for [(H₂N)₃Hf–Ir(CO)₄].

Dedicated to the memory of Professor Jürgen Hinze and published as part of the Hinze Memorial Issue.

A. Krapp · G. Frenking (✉)
Fachbereich Chemie, Philipps-Universität,
Hans-Meerwein-Strasse, 35039 Marburg, Germany
e-mail: frenking@chemie.uni-marburg.de

A. Krapp
Senter for teoretisk og beregningsorientert
kjemi, Kjemisk institutt, Universitetet i Oslo,
Postboks 1033 Blindern, 0315 Oslo, Norway

1 Introduction

The chemistry of metal–metal bonds, which dates back to 1926 when a direct bond between Hg(I) ions was evidenced through an X-ray structure analysis [1] was strongly vitalized since the 1960s when Cotton showed that there were molecules, which even have multiple bonds between metal atoms [2]. A large number of compounds with metal–metal bonds have been synthesized and structurally characterized to date, where the majority of them have M–M bonds between identical metal atoms [3]. Heterodinuclear compounds between different metal atoms M–M′ have become the focus of experimental research in the last two decades because of the potential interest of such species as catalysts in metal-mediated reactions [4–8]. The so-called "early–late" complexes, RₙM–M′Lₘ, play a particular role, in that the early metal M is in a high oxidation state and bonded via electron-sharing bonds to substituents R, while the late metal M′ is in a low oxidation state and bonded via donor–acceptor interactions with the ligands L [6–9]. The M–M′ bond in the compounds may be a single or multiple bond.

Several quantum chemical studies of compounds with metal–metal bonds have been published in the last decade[1] [31], but only few theoretical investigations have dealt with heterodinuclear complexes [12, 31]. We became interested in such compounds through the synthesis and X-ray structure analysis of MeSi{SiMe₂N(4-MeC₆H₄)}₃ M–Co(CO)₄ where M = Ti, Zr, which posed numerous
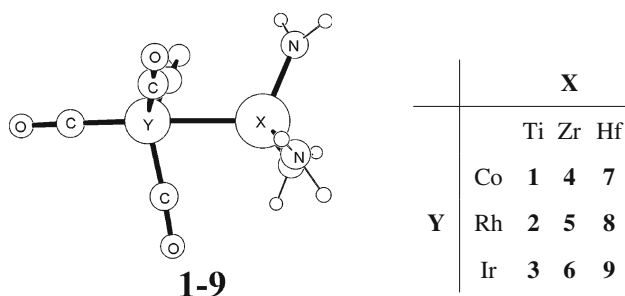
---

[1] Representative examples [10–31].

questions about the description of the bonding situation. The latter compounds were synthesized and the bonding situation in the molecules was analyzed by Jansen et al. [31]. We took this work as a starting point for our ongoing work, which aims at a systematic investigation of the chemical bond in transition metal complexes [32, 33], with the help of the energy decomposition analysis (EDA) [34–36]. To this end, we calculated first the model compound $HSi\{SiH_2NH\}_3M–Co(CO)_4$. However, the focus of this work lies on the calculation of the compounds $(H_2N)_3M–M'(CO)_4$ (M = Ti, Zr, Hf; M' = Co, Rh, Ir) 1–9 (Scheme 1) and on the analysis of the metal–metal bonding situation.

2 Methods

The geometries of the molecules were optimized at the gradient-corrected DFT level of theory using Becke's exchange functional [37] in conjunction with Perdew's correlation functional [38] (BP86). Uncontracted Slater-type orbitals (STOs) were employed as basis functions in SCF calculations [39]. Triple-ζ-quality basis sets were used, which were augmented by two sets of polarization functions, that is, p and d functions for hydrogen atoms and d and f functions for the other atoms. This level of theory is denoted by BP86/TZ2P. An auxiliary set of s, p, d, f and g STOs was used to fit the molecular densities and to represent the Coulomb and exchange potentials accurately in each SCF cycle [40]. Scalar relativistic effects were considered using the zeroth-order regular approximation (ZORA) [41–45]. The vibrational frequencies of the molecules were calculated using analytical derivatives. The calculations were carried out using the ADF(2005.1) program package [46].

In the EDA, bond formation between the interacting fragments is divided into three steps, which can be interpreted in a plausible way. In the first step, the fragments, which are calculated with the frozen geometry of the entire molecule, are superimposed without electronic relaxation yielding the quasiclassical electrostatic attraction ΔE_{elstat}.

Scheme 1

In the second step, the product wave function becomes antisymmetrized and renormalized, which gives the repulsive term ΔE_{Pauli}, termed Pauli repulsion. In the third step, the molecular orbitals relax to their final form to yield the stabilizing orbital interaction ΔE_{orb}. The last term can be divided into contributions of orbitals having different symmetry. This step is crucial for the present study. The sum of the three terms, $\Delta E_{elstat} + \Delta E_{Pauli} + \Delta E_{orb}$, gives the total interaction energy ΔE_{int}:

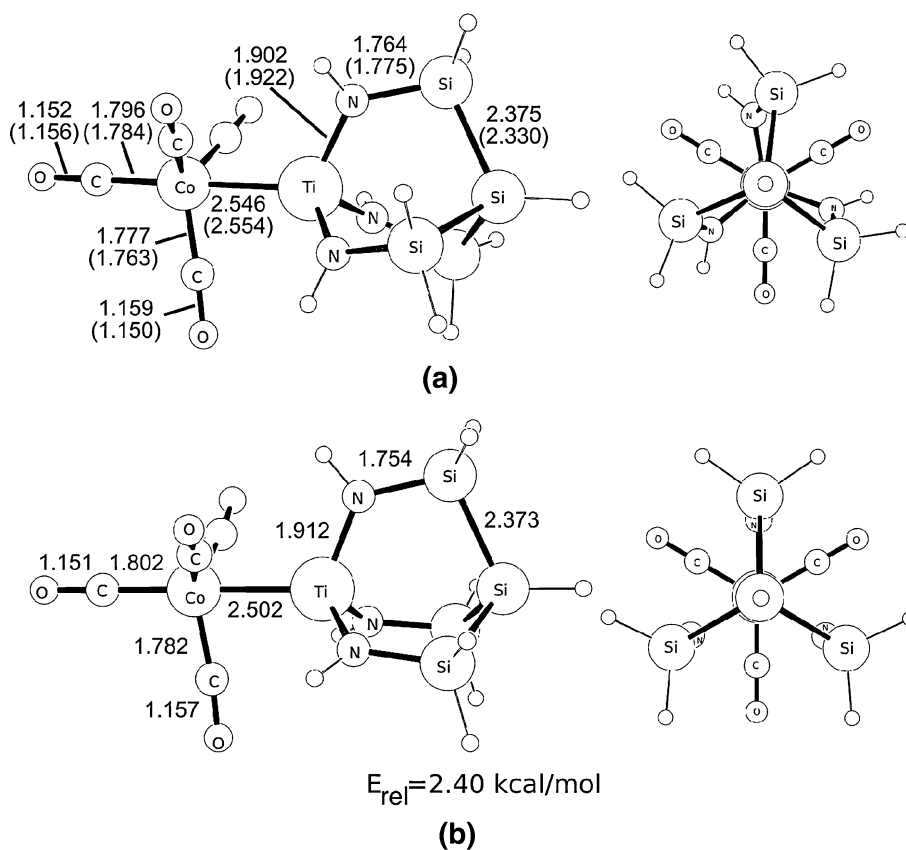$$\Delta E_{int} = \Delta E_{elstat} + \Delta E_{Pauli} + \Delta E_{orb}.$$

The EDA calculations involving open-shell fragments neglect, for technical reasons, the spin polarization in the fragments. This means that the interaction energies ΔE_{int} are slightly larger (in the order of a few kcal/mol per unpaired electron) than those using fully relaxed orbitals. This error has been neglected in the present study, because the small differences are unimportant for the discussion in this study. Further details on EDA can be found in literature [46, 47].

3 Results

We first optimized the geometry of the complex [HSi$(SiH_2NH)_3$Ti–Co(CO)$_4$](M), which is a model for the experimentally observed [31] compound [MeSi{SiMe$_2$N(4-MeC$_6$H$_4$)}$_3$Ti–Co(CO)$_4$] where the substituents at nitrogen and silicon are replaced by hydrogen. Figure 1 shows the calculated structure and the most important bond lengths and angles. The comparison with the experimental data of the real compound shows a very good agreement, which means that the bonding situation in **M** is very similar to that in [MeSi{SiMe$_2$N(4-MeC$_6$H$_4$)}$_3$Ti–Co(CO)$_4$]. The CO groups in the equatorial position of the Co(CO)$_4$ moiety are tilted toward the titanium fragment, which indicates that the π-bonding interaction in the Ti–Co bond is as expected weaker than in the Co–CO$_{trans}$ bond. Note that the Co–CO$_{cis}$ bonds in the experimental and theoretical structure are clearly shorter than the Co–CO$_{trans}$ bond.

The optimized geometry of **M** has C_1 symmetry. The projection along the Ti–Co bond, shown in Fig. 1, indicates that the equilibrium geometry may be considered as a slightly distorted structure, which has C_{3v} symmetry where the Si–N bonds are aligned along the Ti–Co bond. We optimized the geometry of **M** with enforced C_{3v} symmetry and found that the latter species, shown in Fig. 1b, is only 2.4 kcal/mol higher in energy than the energy minimum. Since the EDA calculation of the C_{3v} structure makes it possible to separate the σ and π orbital contributions, we used the latter species for the bonding analysis. However, Fig. 1 shows that the Ti–Co bond in the C_{3v} structure is significantly shorter (2.502 Å) than in the equilibrium

Fig. 1 Optimized geometries at BP86/TZ2P for the equilibrium structure of **M** (C_1 symmetry) and the structure with constrained C_{3v} geometry. Bond lengths are given in Å. Experimental values for the substituted homolog of **M** taken from Ref. [31] are shown in parentheses. Relative energy of the C_{3v} structure with respect to the equilibrium form is given in kcal/mol

(a)

$E_{rel} = 2.40$ kcal/mol

(b)

structure (2.546 Å). We conclude that the conformation of the amino ligands at titanium has a rather strong influence on the Ti–Co bond. This will be addressed in the section below.

Table 1 gives the results of the charge distribution and the Wiberg bond indices for **M**. It becomes obvious that the Ti–Co bond is polarized toward the cobalt atom and that the even more polarized Ti–N bond has a much higher bond order than the Ti–Co bond. There is a small charge donation from the HSi(SiH$_2$NH)$_3$Ti moiety to the Co(CO)$_4$ fragment, which amounts to $0.23e$ in the equilibrium form. A similar finding was reported in the work by Jansen et al. [31]. Table 2 gives the EDA results for the C_1 and C_{3v} structures where the HSi(SiH$_2$NH)$_3$Ti and Co(CO)$_4$ fragments in the respective doublet state were chosen as interacting moieties. The data suggest that the electrostatic and covalent contributions to the Ti–Co interactions, which are given by the ΔE_{elstat} and ΔE_{orb} terms, have nearly the same strength. The EDA values for the C_1 and C_{3v} structures are very similar and it is thus justified to use the results for the latter species as probe for the strength of the σ and π bonding. Table 2 shows that the π orbital interactions in **M** comprise only 12.6% of the ΔE_{orb} term. The e orbital term includes interactions from orbitals which have δ symmetry. However, our previous EDA study of the quadruple bond in Re$_2$Cl$_8$$^{2-}$ has shown that the

Table 1 NBO charges q (in e), Wiberg bond indices $P(X–X')$ for model compound **M** in C_1 and C_{3v} symmetry

Parameter	Symmetry	
	C_1	C_{3v}
$q(Co)$	−0.02	−0.02
$q(Ti)$	1.01	0.99
$q(N)$	−1.22	−1.24
$q[Co(CO)_4]$	−0.23	−0.15
$P(Ti–Co)$	0.32	0.40
$P(Ti–N)$	1.05	1.00

contribution of the orbitals, which have genuine δ symmetry to the ΔE_{orb} term, is negligible [48].

Next, we calculated the structures of the model compounds **1–9** (Scheme 1) and analyzed the M–M′ bonding situation. The parent system (H$_2$N)$_3$Ti–Co(CO)$_4$ (**1**) has been studied in more detail to understand the influence of the conformation of the amino substituents at titanium on the Ti–Co bonding situation. Figure 2 shows the calculated geometries of the equilibrium structure **1** and the structures **1a–d**, which where optimized with frozen torsion angles about the Ti–N bonds. The Newman projections in Fig. 2 show that the lone-pair orbitals at nitrogen in conformation **1a** are aligned parallel to the

Table 2 EDA results for model compound **M** in C_1 and C_{3v} symmetry using the uncharged fragments Ti(NHSiH$_2$)$_3$SiH and Co(CO)$_4$ in the doublet state (^2A in C_1 symmetry and $^2A_1$ in C_{3v} symmetry)

	C_1	C_{3v}
ΔE_{int}	−68.2	−63.5
ΔE_{Pauli}	130.7	121.5
ΔE_{elstat}^a	−100.4 (50.5%)	−91.5 (49.5%)
ΔE_{orb}^a	−98.6 (49.5%)	−93.5 (50.5%)
$\Delta E(a_1)^b$ σ	–	−81.6 (87.3%)
$\Delta E(a_2)^b$	–	−0.2 (0.2%)
$\Delta E(e)^b$ π/δ	–	−11.8 (12.6%)
E_{prep}	7.3	4.3
$-D_e$	−61.0	−59.3

All values in kcal/mol

^{a} The percentage values in parentheses give the contribution to the total attractive interactions, $\Delta E_{elstat} + \Delta E_{orb}$

^{b} The percentage values in parentheses give the contribution to the total orbital interactions, ΔE_{orb}
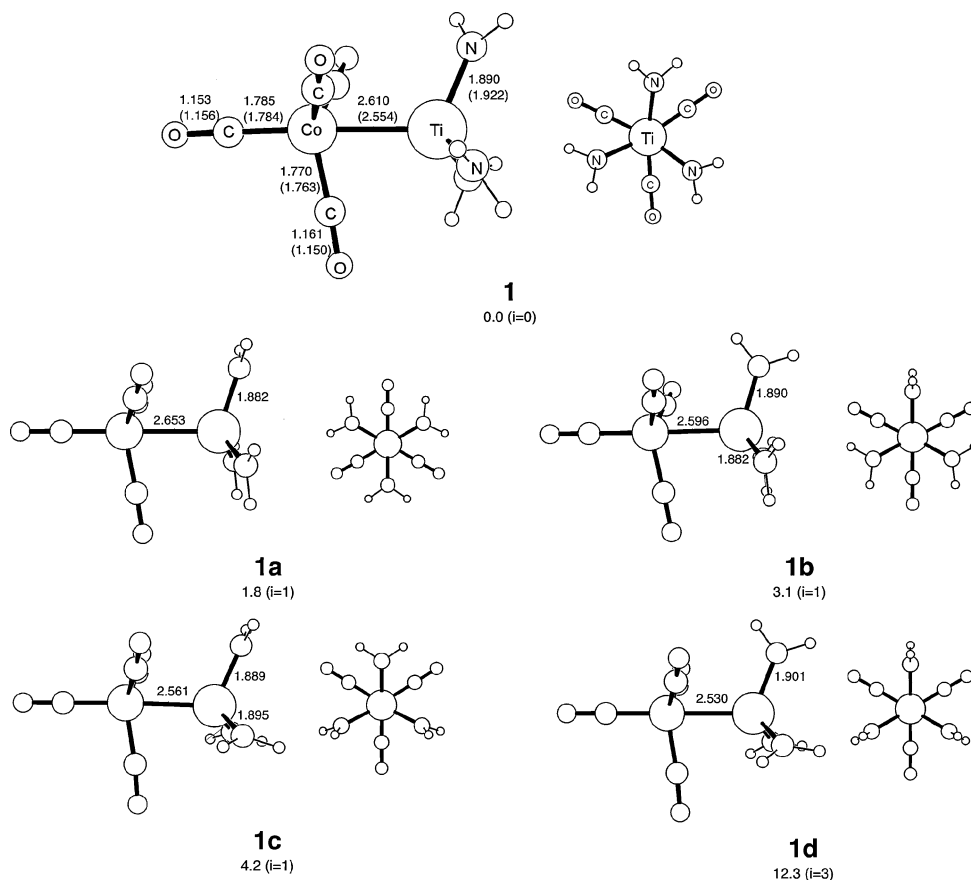
Ti–Co bond and that there is a stepwise rotation of the three amino groups, which leads to the conformations **1b**, **1c**, **1d**. In the latter conformation **1d**, all three lone-pair orbitals of the nitrogen atoms are orthogonal to the Ti–Co bond.

Figure 2 shows that that the Ti–Co bond becomes gradually shorter on rotation of the amino groups in the order **1a** (2.653 Å) → **1b** (2.596 Å) → **1c** (2.561 Å) → **1d** (2.530 Å), while the Ti–N bond length changes only very little. Since the energy of the conformations increases in the same order as the bond length decreases, it follows that the shorter Ti–Co bonds have lower bond dissociation energies (BDEs) and thus are weaker than the longer Ti–Co bonds. The finding that a shorter bond may be weaker than a longer bond has been pointed out before [49]. Figure 3 shows that the change in the Ti–Co distance correlates well with the number of the rotated amino groups. Note that the equilibrium structure **1** has a value, which is between **1a** and **1b**.

Figure 4 shows orbital correlation diagrams for the conformations **1a** and **1d** where the nitrogen lone-pair orbitals are parallel (**1a**) or orthogonal (**1d**) to the Ti–Co bond. Table 3 gives the EDA results for **1**, **1a** and **1b**. The data for the latter two conformations give quantitative information about the strength of the orbital interactions, which are schematically shown in Fig. 4.

Fig. 2 Optimized geometries at BP86/TZ2P for the equilibrium structure of **1** and the conformations **1a**–**1d**, which are calculated with frozen torsion angles of the Ti–NH$_2$ moieties. Bond lengths are given in Å. Experimental values for the substituted homolog of **1** taken from Ref. [31] are shown in parentheses. Relative energies of **1a**–**1d** with respect to **1** are given in kcal/mol. The number of imaginary frequencies i is given after the energy value
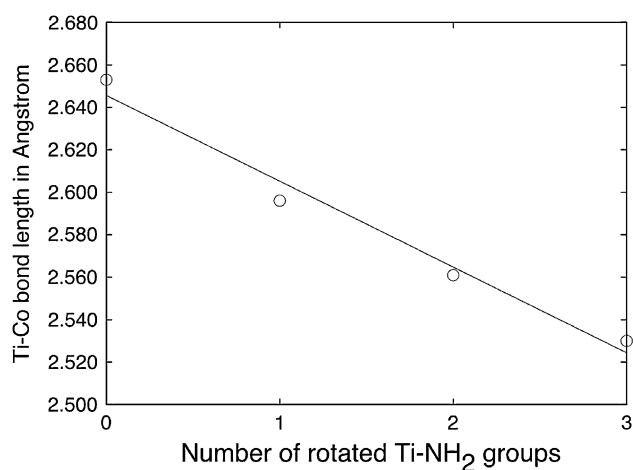
Fig. 3 Plot of the Ti–Co bond length of **1a**–**1d** with respect to the number of rotated Ti–NH$_2$ groups

The EDA results for **1** are very similar to the data for **M** (Table 2), which justifies the use of the former values for the analysis of the bonding situation in the real compound. Note that the interaction energy in **1a** ($\Delta E_{int} = -68.2$ kcal/mol) is only slightly less than in **1** ($\Delta E_{int} = -70.9$ kcal/mol), but that the values for the three energy components differ more. Both attractive interactions, ΔE_{elstat} and ΔE_{orb}, and the repulsive term ΔE_{Pauli} are weaker in **1a** than in **1**, which precludes the identification of a single component as reason for the slightly weaker bonding in the former structure.

The EDA results for the conformations **1a** and **1d** are very interesting. The data show that the total interaction energy in **1d** ($\Delta E_{int} = -65.8$ kcal/mol) is only 2.4 kcal/mol weaker than in **1a** ($\Delta E_{int} = -68.2$ kcal/mol). This means that the substantially higher energy of the former species, which is 10.3 kcal/mol less stable than the latter, comes mainly from the preparation energy of the fragments. Table 3 shows that the calculated value for ΔE_{prep} in **1d** (21.8 kcal/mol) is significantly higher than in **1a** (13.9 kcal/mol). The energy difference between **1a** and **1d** is thus mainly determined by the intra-fragment interactions and less by the bonding between the fragments.

It is interesting to compare the orbital interaction diagram shown in Fig. 4 with the EDA results in Table 3. The data show that the slightly weaker orbital interactions in **1d** compared with **1a** come from the σ orbitals, while the π bonding in the former conformations is even stronger (-10.1 kcal/mol) than in the latter (-6.9 kcal/mol). The orbital interaction diagram allows for an interpretation of this effect, since it becomes clear how the rotation of the amine groups effects both the σ- and π orbitals of the Ti(NH$_2$)$_3$ fragment. In **1a**, the lone pairs of the NH$_2$-groups overlap positively with the σ-bonding d_{z2}-orbital ($1a_1$) and the π-bonding d_{yz}- and d_{xz}-orbitals ($1e$) of Ti, whereas in **1d**

the lone pairs on N cannot overlap with the σ- and π-orbitals on Ti and mix only with orbitals of δ-symmetry ($1\,e$ in Fig. 4b). The delocalization of the N-lone pair density into the π-orbitals of Ti in **1a** leads to a weakening of the Co–Ti π-bond, since the $2\,e$ orbital in **1a** gets a Co–Ti π-antibonding character. On the other hand, the rotation of the N-lone pairs leads to a partial depopulation of the Ti d_{z2}-orbital in **1d**, which results in a stabilization of the $1\,a_1$ orbital of the Ti(NH$_2$)$_3$ fragment. Thereby, the tendency for partial charge transfer out of this orbital from Ti to Co, which is necessary for the formation of the polar Ti–Co σ bond, is reduced.

The optimized equilibrium structures of **2**–**9** at BP86/TZ2P are very similar to the calculated geometry of **1** except for (H$_2$N)$_3$Hf–Rh(CO)$_4$ (**8**) where the optimization yielded a structure where one CO ligand is in a bridging position between the metal atoms. The geometry optimization of **8** at BP86 with Gaussian 98 using a DZP quality basis set,[2] which was proven to provide accurate geometries for transition metal compounds [53–57], gave an optimized structure without a bridging CO ligand (as given).[3] Table 4 gives the optimized M–M′ bond lengths, the theoretically predicted BDEs and the results of the charge partitioning analysis.

The calculations predict that the M–M′ bond strength significantly increases when the group 4 element becomes heavier, Ti < Zr < Hf. The differences between the BDEs of the group 9 elements M′ (Co, Rh, Ir) for a given atom M are smaller. The strongest M–M′ bond is predicted for (H$_2$N)$_3$Hf–Ir(CO)$_4$ (**9**). The group 4 elements carry a large positive charge, which strongly increases with Ti < Zr < Hf, while the partial charge at atom M′ changes very little (Table 4). The calculated charge distribution could be taken as a sign for a larger electrostatic contribution to the M–M′ bonds. Note that the bond order P(M–M′) decreases when M becomes heavier.

We analyzed the nature of the M–M′ bonds in **1**–**9** with the EDA method. The results are given in Table 5. The EDA data support the conclusion that the M–M′ bonds of the heavier group 4 elements Zr and Hf have a larger electrostatic character than the titanium compounds. A

---

[2] For the transition metals, we used small-core effective core potentials [50] in combination with the contracted valence basis set [441/211(N-1)1] as described in: [51]; the basis set for the main group atoms is the standard Pople basis 6-31G(d) as implemented in Gaussian98: Gaussian 98 (Revision A.7), [52].

[3] The use of the BP86/DZP (GTOs) geometry of **8** does not mean that we consider the geometries at this level of theory to be in better agreement with experiment than the structures which are predicted at BP86/TZ2P (STOs). Compound **8** is a model for the real system which has bulky substituents that prevent ligand bridging. We use the BP86/DZP optimized geometry of **8** because it does not give a structure with a bridging CO ligand.

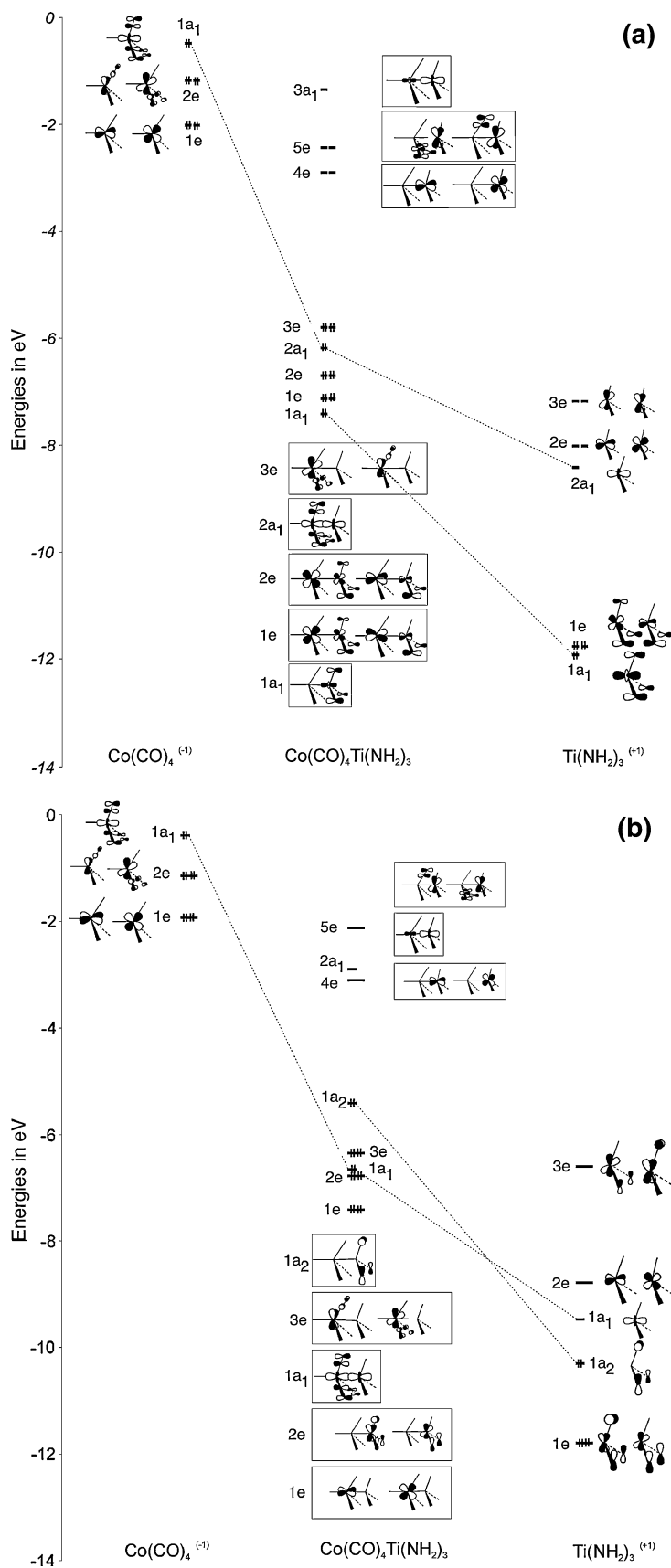**Fig. 4** Orbital correlation
diagram for (**a**) **1a** and (**b**) **1d**

Table 3 EDA results for compounds **1**, **1a** and **1d**

	1 $Ti(NH_2)_3^{(0)}$ $Co(CO_4)^{(0)}$	**1a** $Ti(NH_2)_3^{(0)}$ $Co(CO_4)^{(0)}$	**1d** $Ti(NH_2)_3^{(0)}$ $Co(CO_4)^{(0)}$
ΔE_{int}	−70.9	−68.2	−65.8
ΔE_{Pauli}	135.8	125.1	125.7
ΔE_{elstat}^a	−106.5 (51.5%)	−98.3 (50.9%)	−97.9 (51.1%)
ΔE_{orb}^a	−100.1 (48.5%)	−94.9 (49.1%)	−93.6 (48.9%)
$\Delta E(a_1)^b$ σ	–	−88.0 (92.8%)	−83.3 (89.0%)
$\Delta E(a_2)^b$	–	0.0 (0.0%)	−0.2 (0.2%)
$\Delta E(e)^b$ π/δ	–	−6.9 (7.2%)	−10.1 (10.8%)
E_{prep}	14.8	13.9	21.8
$-D_e$	−56.1	−54.3	−44.0

Energy values in kcal/mol

[a] The percentage values in parentheses give the contribution to the total attractive interactions, $\Delta E_{elstat} + \Delta E_{orb}$

[b] The percentage values in parentheses give the contribution to the total orbital interactions, ΔE_{orb}

Table 4 Calculated (BP86/TZ2P) bond lengths R(M–M′) (in Å), bond dissociation energies D_e of the M–M′ bond (in kcal/mol), NBO charges q (in e) and Wiberg bond orders P(M–M′) of compounds **1–9**

Compound (M–M′)	R(M–M′)	D_e	q(M)	q(M′)	q[M(NH_2)_3]	P(M–M′)
1 (Ti–Co)	2.610	56.1	1.02	−0.03	0.35	0.27
2 (Ti–Rh)	2.725	56.4	1.07	0.01	0.35	0.33
3 (Ti–Ir)	2.801	59.4	1.08	0.26	0.36	0.30
4 (Zr–Co)	2.754	66.2	1.64	−0.05	0.43	0.22
5 (Zr–Rh)	2.864	66.2	1.65	−0.03	0.41	0.27
6 (Zr–Ir)	2.916	69.3	1.66	0.22	0.42	0.26
7 (Hf–Co)	2.710	71.6	1.81	−0.06	0.43	0.21
8 (Hf–Rh)	2.833[a]	74.3[a]	1.81	−0.03	0.42	0.26
9 (Hf–Ir)	2.882	75.7	1.82	0.20	0.42	0.25

[a] Using a BP86/DZP optimized geometry; see text

correlation between atomic partial charges and electrostatic character is not generally valid. Atomic partial charges do not give any information about the spatial distribution of the electronic charge. It has been shown that the anisotropy of the electronic charge, which belongs to an atomic basin, is much more important for the electrostatic interaction between two atoms than their partial charges [58]. The spatial distribution of the charge density in **1**–**9** is very similar and thus the changes in the electrostatic interactions for the molecules are mainly determined by the different electronegativities. This is the reason that the atomic partial charges and the contribution of ΔE_{elstat} to the M–M′ attraction have the same trend.

4 Summary and conclusion

The results of this work can be summarized as follows. The Ti–Co bond in the molecule $[HSi(SiH_2NH)_3Ti–Co(CO)_4]$, which is a model for the experimentally observed compound $[MeSi\{SiMe_2N(4-MeC_6H_4)\}_3Ti–Co(CO)_4]$, has a theoretically predicted BDE of $D_e = 59.3$ kcal/mol. The bonding analysis suggests that the titanium atom carries a large positive charge, while the cobalt atom is nearly neutral. The covalent and electrostatic contributions to the Ti–Co attraction have similar strength. The Ti–Co bond can be classified as a polar single bond, which has only little π contribution. Calculations of the model compound $[(H_2N)_3Ti–Co(CO)_4]$ show that the rotation of the amino groups has a very large influence on the length and on the strength of the Ti–Co bond. The M–M′ bond in the series $[(H_2N)_3M–M'(CO)_4]$ (M = Ti, Zr, Hf; M′ = Co, Rh, Ir) becomes clearly stronger with Ti < Zr < Hf, while the differences between the bond strengths due to change of the atoms M′ are much smaller. The strongest M–M′ bond is predicted for $[(H_2N)_3Hf–Ir(CO)_4]$.

Table 5 EDA results for compounds **1–9**

	1 $(NH_2)_3Ti^{(0)}$ $Co(CO)_4^{(0)}$	**2** $(NH_2)_3Ti^{(0)}$ $Rh(CO)_4^{(0)}$	**3** $(NH_2)_3Ti^{(0)}$ $Ir(CO)_4^{(0)}$	**4** $(NH_2)_3Zr^{(0)}$ $Co(CO)_4^{(0)}$	**5** $(NH_2)_3Zr^{(0)}$ $Rh(CO)_4^{(0)}$	**6** $(NH_2)_3Zr^{(0)}$ $Ir(CO)_4^{(0)}$	**7** $(NH_2)_3Hf^{(0)}$ $Co(CO)_4^{(0)}$	**9** $(NH_2)_3Hf^{(0)}$ $Ir(CO)_4^{(0)}$
ΔE_{int}	−70.9	−70.2	−72.3	−79.3	−79.0	−79.2	−81.8	−83.7
ΔE_{Pauli}	135.8	131.4	131.6	168.1	163.8	162.8	178.8	175.2
ΔE_{elstat}^a	−106.5 (51.5%)	−112.8 (55.9%)	−115.7 (56.7%)	−132.1 (53.4%)	−142.1 (58.5%)	−143.5 (59.3%)	−140.3 (53.8%)	−155.0 (59.9%)
ΔE_{orb}^a	−100.1 (48.5%)	−88.8 (44.1%)	−88.2 (43.3%)	−115.2 (46.6%)	−100.6 (41.5%)	−98.5 (40.7%)	−120.3 (46.2%)	−103.9 (40.1%)
E_{prep}	14.8	13.8	12.9	13.1	12.8	10.0	10.2	8.0
$-D_e$	−56.1	−56.4	−59.4	−66.2	−66.2	−69.3	−71.6	−75.7

Energy values in kcal/mol

[a] The percentage values in parentheses give the contribution to the total attractive interactions, $\Delta E_{elstat} + \Delta E_{orb}$

References

1. Havighurst RJ (1926) J Am Chem Soc 48:2113
2. Cotton FA, Harris CB (1965) Inorg Chem 4:330
3. Cotton FA, Murillo CA, Walton RA (eds) (2005) Multiple bonds between metal atoms, 3rd edn. Springer Science and Business Media, Inc, New York
4. Braunstein P, Rose J (1995) In: Abel EW, Stone FGA, Wilkinson G (eds) Comprehensive organometallic chemistry II: a review of the literature 1982–1994, vol 10. Pergamon, New York, p 351
5. Chetcuti MJ (1995) In: Abel EW, Stone FGA, Wilkinson G (eds) Comprehensive organometallic chemistry II: a review of the literature 1982–1994, vol 10. Pergamon, New York, p 23
6. Wheatley N, Kalck P (1999) Chem Rev 99:3379
7. Gade LH (2000) Angew Chem Int Ed 39:2658
8. Gade LH (2000) Angew Chem 112:2768
9. Stephan DW (1989) Coord Chem Rev 95:41
10. Wiest R, Strich A, Bénard M (1991) New J Chem 15:801
11. Xu Z, Lin Z (1998) Chem Eur J 4:28
12. Wada T, Nishio S, Yada T, Hayashi S, Matsuzaki A, Sato H, Kobayashi H, Yamabe T (2001) J Mol Struct (Theochem) 543:65
13. Petrie S, Stranger R (2004) Inorg Chem 43:2597
14. Cavigliasso G, Kaltsoyannis N (2006) Inorg Chem 45:6828
15. Cavigliasso G, Kaltsoyannis N (2006) Dalton Trans 5476
16. Saito K, Nakao Y, Sato H, Sakaki S (2006) J Phys Chem A 110:9710
17. Kreisel KA, Yap GPA, Dmitrenko O, Landis CR, Theopold KH (2007) J Am Chem Soc 129:14162
18. Cavigliasso G, Kaltsoyannis N (2007) Inorg Chem 46:3557
19. Roos BO, Borin AC, Gagliardi L (2007) Angew Chem Int Ed 46:1469
20. Roos BO, Borin AC, Gagliardi L (2007) Angew Chem 119:1491
21. La Macchia G, Gagliardi L, Power PP, Brynda M (2008) J Am Chem Soc 130:5104
22. La Macchia G, Aquilante F, Veryazov V, Roos BO, Gagliardi L (2008) Inorg Chem 47:11455
23. Noor A, Wagner FR, Kempe R (2008) Angew Chem Int Ed 47:7246
24. Noor A, Wagner FR, Kempe R (2008) Angew Chem 120:7356
25. Hsu CW, Yu JSK, Yen CH, Lee GH, Wang Y, Tsai YC (2008) Angew Chem Int Ed 47:9933
26. Hsu CW, Yu JSK, Yen CH, Lee GH, Wang Y, Tsai YC (2008) Angew Chem 120:10081
27. Horvath S, Gorelsky SI, Gambarotta S, Korobkov I (2008) Angew Chem Int Ed 47:9937
28. Horvath S, Gorelsky SI, Gambarotta S, Korobkov I (2008) Angew Chem 120:10085
29. Poineau F, Gagliardi L, Forster PM, Sattelberger AP, Czerwinski KR (2009) Dalton Trans 5954
30. Hyla-Kryspin I, Grimme S, Djukic JP (2009) Organometallics 28:1001
31. Jansen G, Schubart M, Findeis B, Gade LH, Scowen IJ, McPartlin M (1998) J Am Chem Soc 120:7239
32. Frenking G, Wichmann K, Fröhlich N, Loschen C, Lein M, Frunzke J, Rayón VM (2003) Coord Chem Rev 238–239:55
33. Lein M, Frenking G (2005) In: Dykstra CE, Frenking G, Kim KS, Scuseria GE (eds) Theory and applications of computational chemistry: the first 40 years. Elsevier, Amsterdam, p 367
34. Ziegler T, Rauk A (1979) Inorg Chem 18:1558
35. Ziegler T, Rauk A (1979) Inorg Chem 18:1755
36. Morokuma K (1971) J Chem Phys 55:1236
37. Becke AD (1988) Phys Rev A 38:3098
38. Perdew JP (1986) Phys Rev B 33:8822
39. Snijders JG, Baerends EJ, Vernooijs P (1982) At Nucl Data Tables 26:483
40. Krijn J, Baerends EJ (1984) Fit functions in the HFS method, Internal Report (in Dutch), Vrije Universiteit Amsterdam, The Netherlands
41. Chang C, Pelissier M, Durand P (1986) Phys Scr 34:394
42. Heully JL, Lindgren I, Lindroth E, Lundqvist S, Mårtensson-Pendrill AM (1986) J Phys B 19:2799
43. van Lenthe E, Baerends EJ, Snijders JG (1993) J Chem Phys 99:4597
44. van Lenthe E, Snijders JG, Baerends EJ (1996) J Chem Phys 105:6505
45. van Lenthe E, van Leeuwen R, Baerends EJ, Snijders JG (1996) Int J Quantum Chem 57:281
46. te Velde G, Bickelhaupt FM, Baerends EJ, Fonseca Guerra C, van Gisbergen SJA, Snijders JG, Ziegler T (2001) J Comput Chem 22:931
47. Bickelhaupt FM, Baerends EJ (2000) Rev Comput Chem 15:1
48. Krapp A, Lein M, Frenking F (2008) Theor Chem Acc 120:313
49. Frenking G, Wichmann K, Fröhlich N, Grobe J, Golla W, Le Van D, Krebs B, Läge M (2002) Organometallics 21:2921
50. Hay PJ, Wadt WR (1985) J Chem Phys 82:299
51. Frenking G, Antes I, Böhme M, Dapprich S, Ehlers AW, Jonas V, Neuhaus A, Otto M, Stegmann R, Veldkamp A, Vyboishchikov SF (1996) Rev Comp Chem 8:63
52. Frisch MJ, Trucks GW, Schlegel HB, Scuseria GE, Robb MA, Cheeseman JR, Zakrzewski VG, Montgomery JA Jr, Stratmann RE, Burant JC, Dapprich S, Millam JM, Daniels AD, Kudin KN, Strain MC, Farkas O, Tomasi J, Barone V, Cossi M, Cammi R, Mennucci B, Pomelli C, Adamo C, Clifford S, Ochterski J, Petersson GA, Ayala PY, Cui Q, Morokuma K, Malick DK, Rabuck AD, Raghavachari K, Foresman JB, Cioslowski J, Ortiz JV, Baboul AG, Stefanov BB, Liu G, Liashenko A, Piskorz P, Komaromi I, Gomperts R, Martin RL, Fox DJ, Keith T, Al-Laham MA, Peng CY, Nanayakkara A, Gonzalez C, Challacombe M, Gill BG, Johnson PMW, Chen W, Wong MW, Andres JL, Head-Gordon M, Replogle ES, Pople JA (1998) Gaussian, Inc., Pittsburgh, PA
53. Neuhaus A, Veldkamp A, Frenking G (1994) Inorg Chem 33:5278
54. Antes I, Frenking G (1995) Organometallics 14:4263
55. Dapprich S, Frenking G (1996) Organometallics 15:4547
56. Vyboishchikov SF, Frenking G (1998) Chem Eur J 4:1439
57. Lupinetti AJ, Jonas V, Thiel W, Strauss SH, Frenking G (1999) Chem Eur J 5:2573
58. Uddin J, Frenking G (2001) J Am Chem Soc 123:1683